

# Breast Density Assessment Using Wavelet Features on Mammograms

Frank Schebesch<sup>1,\*</sup>, Mathias Unberath<sup>1,2,\*</sup>, Ingwer Andersen<sup>1</sup>,  
Andreas Maier<sup>1,2</sup>

<sup>1</sup>Pattern Recognition Lab, FAU Erlangen-Nürnberg, Germany

<sup>2</sup>Graduate School in Advanced Optical Technologies, Erlangen, Germany

\*Both authors are co-first authors listed in alphabetical order.

`frank.schebesch@fau.de`

**Abstract.** Breast density differs from almost entirely fatty to extremely dense tissue composition. In mammography screenings, physicians are often supported by computer-aided detection and diagnosis systems (CAD) whose detection rate is affected by the density of the breast. An automatic pre-assessment of breast density would enable a specific analysis adapted to each density class. Digital mammograms from the INbreast database [1] are decomposed into Haar-Wavelet components and several levels are used for classification. A random forest classifier is applied on the averaged Wavelet components for four class densities which yields an accuracy of 64.53% in CC-view and 51.22% in MLO-view. The 3-class problem with a combined class of medium densities yields an accuracy of 73.89% in CC-view and 67.80% in MLO-view.

## 1 Introduction

Breast cancer is one of the most common cancers in women. Early detection increases the chances of successful treatment and decreases the mortality rate. However, depending on age and anatomy the density of the breast differs from almost entirely fatty to extremely dense tissue composition making every breast unique. Pathological findings which mostly have a higher density than the parenchyma can be obscured by surrounding tissue. Physicians usually take special care in mammography screenings for women with dense breasts, i.e. additional imaging or more frequent screenings. CAD is intended to support the physician in detection of lesions in and diagnosis of the mammograms [2]. The digital images are computationally analyzed for abnormalities and the findings are presented as a second opinion to the physician. But these systems are also subject to detection difficulties related to dense (healthy) tissue overlaying actual lesions. The sensitivity of such a system can drop significantly as the overall breast density increases [3] and differences in breast density may have a non-negligible effect on the detection of malignant masses [4]. To our knowledge, in CAD feature computation is utilized without explicit adaptation to the underlying breast density class, although a differentiated treatment might improve detection results. In this work an algorithmic approach for prior assessment of breast density is shown to enable specific processing for each class of breast density.

## 2 Materials and Methods

Manual and semi-automated methods are known to estimate the breast density in mammograms, one of which is integration of a circumscribed tissue area using a planimeter. Others involve computerized thresholding to separate dense from non-dense regions [5]. While these demand the physician’s input, an automated approach was suggested for screen-film mammography, which includes noise filtering and statistical evaluation of the downsampled breast image [6]. It showed only moderate Spearman correlation with the BI-RADS density assessment standard. Instead of directly estimating density percentage, the method described here uses an algorithm that is trained on BI-RADS density scores.

### 2.1 Mammographic data and BI-RADS report

Up to date, digital mammography is the standard acquisition method to detect breast cancer in women. In a usual screening each breast is scanned from two different views, cranio-caudal (CC) and mediolateral oblique (MLO). The physician compares both breasts in structure and tissue composition and looks for pathologies in both views. For reliable and standardized transfer of a diagnosis, e.g. to another physician or a follow-up screening, the BI-RADS reporting system (Breast Imaging Reporting and Data System [7]) is the most commonly used. Therein different types of breast are categorized and all known findings are described in detail. It also defines how to determine the final BI-RADS score (from 0 to 6) which reflects the severity of the findings for each breast and thus leads either to follow-up treatment if found malignant or a relief of the patient if found benign. Breast density is divided into four classes: almost entirely fatty, scattered areas of fibroglandular density, heterogeneously dense, and extremely dense. Below these are denoted by ACR 1–4 (**Fig. 1**).

The INbreast database [1] is a publicly available database of digital mammograms (FFDM) which includes 115 pathological cases and a total of 410 images. Full reports of the findings including the BI-RADS score and the type of breast density are provided. The image data from this database was used for feature computation and the expert annotations allowed unambiguous class labels.

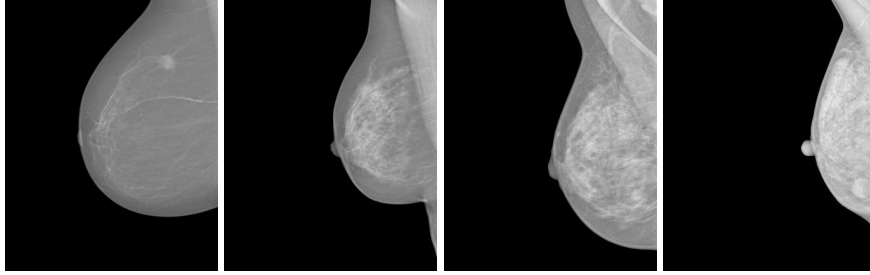
### 2.2 2-D Haar-Wavelet analysis of gray level images

The ACR density classes differ in amount of absorbed energy and density patterns. Intensity integration does not fully take into account the information given by dense structures. Using the Haar-Wavelet transform, density patterns on multiple scales can be extracted and different frequencies and amounts of dense tissue can be retrieved.

The Wavelet decomposition originates from a system of orthogonal functions proposed by Haar [8] which consists of the father wavelet  $\chi_0^0$  and the family of step functions  $(\chi_i^n)_{i=1, \dots, 2^n-1}^{n \in \mathbb{N}}$  on the interval  $[0, 1)$  with

$$\chi_0^0 \equiv 1, \quad \chi_i^n(x) = \begin{cases} \sqrt{2^{n-1}}, & x \in \left[ \frac{2(i-1)}{2^n}, \frac{2i-1}{2^n} \right), \\ -\sqrt{2^{n-1}}, & x \in \left[ \frac{2i-1}{2^n}, \frac{2i}{2^n} \right). \end{cases}$$

**Fig. 1.** From left to right different breast densities in mammograms: almost entirely fatty (ACR 1), scattered areas of fibroglandular density (ACR 2), heterogeneously dense (ACR 3), and extremely dense (ACR 4).



This scheme can easily be extended to higher dimensions using the product space  $X \times X$  where  $X := \bigcup_{i=1, \dots, 2^{n-1}} \{\chi_i^n\} \cup \{\chi_0^0\}$ . The decomposition of a continuous image  $f : [0, 1]^2 \rightarrow U \subset \mathbb{R}$  is then given by

$$f(x, y) \propto \sum_{\chi, \chi' \in X} f_{\chi\chi'} \chi(x) \chi'(y), \quad (1a)$$

$$f_{\chi\chi'} := \int_0^1 \int_0^1 f(x, y) \chi(x) \chi'(y) dx dy, \quad \forall \chi, \chi' \in X. \quad (1b)$$

The proportionality factor in (1a) is the mean value of  $f$ .

Let  $K = 2^\kappa$ ,  $L = 2^\lambda$ ,  $\kappa, \lambda \in \mathbb{N}$ , be the dimensions of a given digital image  $g = (g_{k,l})_{k,l} \in \mathbb{R}^{K \times L}$ . For an arbitrary image this can be achieved by either resizing or zero-padding. Then the decomposition into Haar-Wavelet components  $(g_{k,l}^{n,m})_{k=1, \dots, 2^n}^{l=1, \dots, 2^m}$ ,  $n = 1, \dots, \kappa$ ,  $m = 1, \dots, \lambda$  can be computed straightforwardly by setting

$$g_{k,l}^{\kappa,\lambda} = g_{k,l}, \quad k = 1, \dots, K, \quad l = 1, \dots, L,$$

and first applying the 1-D decomposition along the rows

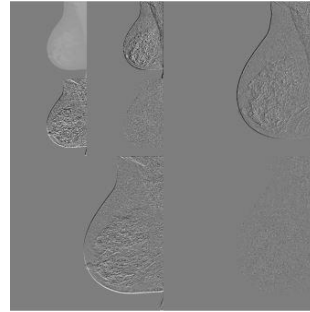
$$g_{k,l}^{n,m-1} = \frac{1}{\sqrt{2}}(g_{k,2l-1}^{n,m} + g_{k,2l}^{n,m}), \quad l = 1, \dots, 2^{m-1}, \quad m = 1, \dots, \lambda,$$

$$g_{k,l+2^{m-1}}^{n,m-1} = \frac{1}{\sqrt{2}}(g_{k,2l-1}^{n,m} - g_{k,2l}^{n,m}), \quad l = 1, \dots, 2^{m-1}, \quad m = 1, \dots, \lambda,$$

and then analogously along the columns of each component of the row-wise decomposition. Additionally the lower level components from the father wavelet of each dimension are given by

$$g_{0,0}^{0,0} := \frac{1}{KL} \sum_{l,k=1}^{K,L} g_{k,l}, \quad g_{0,l}^{0,m} := \frac{1}{K} \sum_{k=1}^K g_{k,l}^{\kappa,m}, \quad g_{k,0}^{n,0} := \frac{1}{L} \sum_{l=1}^L g_{k,l}^{n,\lambda}.$$

**Fig. 2.** Example for two levels of the wavelet decomposition. Every subsequent level is shown in the top left, all others are difference images. On the bottom left and top right one finds the directional information w.r.t. the axes, and on the diagonal the different levels of diagonal gradients. On the top left the summation image of the lowest level can be seen.



In **Fig. 2** two levels of the Wavelet features are shown for a breast in MLO-view. On lower levels of the decomposition, i.e. those from Haar basis functions with larger support, the structures of the glandular tissue become dominant for the denser breasts.

### 2.3 Density classification using WEKA

A random forest classifier [9] with 300 iterations from the WEKA toolbox [10] was used to determine the density of the breast from the mammograms. Since more classes increase the difficulty of solving the classification problem, breast density classes were tested in two ways. First all four ACR classes ACR 1–4 were considered. In a second approach three classes were chosen as “fatty” (ACR 1), “glandular” (ACR 2–3), and “dense” (ACR 4). Features were computed as the average of each summation and difference image over eight levels of the Wavelet decomposition reflecting the energy contained in dense structures on multiple scales. Since the summation image is included, this means that the overall energy in the image is also included. For estimation of the classification quality a leave-one-out cross-validation was performed.

## 3 Results

A total of 203 images showing left and right breasts in CC-view were extracted from the INbreast database divided into 67 images of class ACR 1, 73 images of

ACR	1	2/3	4
1	43	24	0
2/3	16	104	2
4	0	11	3

**Table 1.** Confusion matrix for the 3-class problem in CC-view. Accuracy was 73.89% with an average AuROC of 0.83.

ACR	1	2/3	4
1	39	30	0
2/3	21	98	3
4	0	12	2

**Table 2.** Confusion matrix for the 3-class problem in MLO-view. Accuracy was 67.80% with an average AuROC of 0.77.

**Table 3.** Confusion matrix for the 4-class problem in CC-view. Accuracy was 64.53% with an average AuROC of 0.80. **Table 4.** Confusion matrix for the 4-class problem in MLO-view. Accuracy was 51.22% with an average AuROC of 0.74.

ACR	1	2	3	4
1	51	14	2	0
2	16	44	11	2
3	5	12	31	1
4	0	4	5	5

ACR	1	2	3	4
1	42	25	2	0
2	24	35	12	2
3	7	15	26	1
4	0	6	6	2

class ACR 2, 49 images of class ACR 3, and 14 of class ACR 4. For MLO-view a total of 205 images divided into 69, 73, 49, and 14 images of the respective classes were taken into account.

**Tab. 1** shows the confusion matrix for the 3-class problem using all CC-view FFDMs and a combined total of 122 images for the “glandular” class. 73.89% of the data was correctly classified and as can be seen in the table there is a relatively high percentage of misclassifications on part of the highest density class. In total the classifier performance for this problem was estimated with a value of 0.83 of the area under the ROC curve (AuROC) averaged over all classes. In case of the 4-class problem for CC-view the confusion matrix in **Tab. 3** shows a slightly better classification of the ACR 1 and ACR 4 classes, but the misclassification of the mixed tissue classes is higher which reflects in an accuracy of 64.53% and an average AuROC of 0.80.

Conducting the same experiment on the MLO-view images as can be seen in **Tab. 2** and **Tab. 3** a similar trend is revealed. The overall classification performance, however, was worse. 67.80% and 51.22% of the 205 instances were correctly classified using three and all four classes, yielding average AuROC values of 0.77 and 0.74, respectively.

## 4 Discussion

Breast density assessment is an important step in screenings for breast cancer. Denser tissue can overlay pathological structures and can make lesion detection more difficult. The results show that classification accuracies up to 73.89% for the three and 64.53% for the four class problem can be achieved when using average features from several Wavelet components. Exclusion of the highest Wavelet components did not seem to have a great impact on this result. While this approach was only tested for the 3-class problem and CC-view images, the outcome suggested that the density information may already be contained in lower levels in the Wavelet decomposition.

The quantitative differences in classification between CC- and MLO-view images are related to the fact that in the latter the pectoral muscle invades the texture of the mammogram, introducing a source of irritation due to its higher

density compared to the breast parenchyma. Additional segmentation would probably improve the classification rate.

The authors are aware of a recent study which shows that CAD-systems as they were available in the period of 2003–2009 had no significant effect on screening performance [11]. Another study indicates that breast density affects CAD-performance for masses, but not for microcalcifications [4]. In both studies CAD is used as a fixed tool which does not take any adaptive behaviour of the system into account. This initial investigation of breast density assessment from FFDMs renders a selective approach possible where for each breast density a specific CAD-analysis is performed. Both sensitivity as well as specificity could be affected. In order to improve the method itself regional labels might prove useful, allowing a very localized feature analysis on several tissue patches.

## Acknowledgment

The authors gratefully acknowledge funding of the Erlangen Graduate School in Advanced Optical Technologies (SAOT) by the German Research Foundation (DFG) in the framework of the German excellence initiative.

## References

1. Moreira IC, Amaral I, Domingues I, et al. INbreast: Toward a Full-field Digital Mammographic Database. *Acad Radiol.* 2012;19(2):236–248.
2. Tang J, Rangayyan RM, Xu J, et al. Computer-Aided Detection and Diagnosis of Breast Cancer with Mammography: Recent Advances. *IEEE Trans Inf Technol Biomed.* 2009;13(2):236–251.
3. Ho WT, Lam PWT. Clinical Performance of Computer-assisted Detection (CAD) System in Detecting Carcinoma in Breasts of Different Densities. *Clin Radiol.* 2003;58(2):133–136.
4. Malich A, Fischer DR, Facius M, et al. Effect of Breast Density on Computer Aided Detection. *J Digit Imaging.* 2005;18(3):227–233.
5. Yaffe MJ. Mammographic Density: Measurement of Mammographic Density. *Breast Cancer Res.* 2008;10(3).
6. Heine JJ, Carston MJ, Scott CG, et al. An Automated Approach for Estimation of Breast Density. *Cancer Epidemiol Biomarkers Prev.* 2008;17(11):3090–3097.
7. D’Orsi CJ, Sickles EA, Mendelson EB, et al. ACR BI-RADS<sup>®</sup> Atlas, Breast Imaging Reporting and Data System. Reston, VA: Am Coll Radiol; 2013.
8. Haar A. On the Theory of Orthogonal Function Systems. In: Heil C, Walnut DF, editors. *Fundamental Papers in Wavelet Theory.* Princeton: Princeton University Press; 2006. p. 155–188.
9. Breiman L. Random Forests. *Mach Learn.* 2001;45(1):5–32.
10. Hall M, Frank E, Holmes G, et al. The WEKA Data Mining Software: An Update. *SIGKDD Explorations.* 2009;11(1):10–18.
11. Lehman CD, Wellman RD, Buist DSM, et al. Diagnostic Accuracy of Digital Screening Mammography with and without Computer-aided Detection. *JAMA Internal Medicine.* 2015; p. 1–10.